Mon. Not. R. Astron. Soc. **394,** 1991–2000 (2009) doi:10.1111/j.1365-2966.2009.14440.x

Near-infrared bulge–disc correlations of lenticular galaxies

Sudhanshu Barway,[1,2]★ Yogesh Wadadekar,[3] Ajit K. Kembhavi[2] and Y. D. Mayya[4]

[1]*South African Astronomical Observatory, PO Box 9, 7935, Observatory, Cape Town, South Africa*
[2]*Inter University Centre for Astronomy and Astrophysics, Post Bag 4, Ganeshkhind, Pune 411 007, India*
[3]*National Centre for Radio Astrophysics, Post Bag 3, Ganeshkhind, Pune 411007, India*
[4]*Instituto Nacional de Astrofisica, Optica y Electronica, Luis Enrique Erro 1, Tonantzintla, Apdo Postal 51 y 216, C.P. 72000, Puebla, Mexico*

Accepted 2008 December 23. Received 2008 December 9; in original form 2008 July 1

ABSTRACT

We consider the luminosity and environmental dependence of structural parameters of lenticular galaxies in the near-infrared *K* band. Using a 2D galaxy image decomposition technique, we extract bulge and disc structural parameters for a sample of 36 lenticular galaxies observed by us in the *K* band. By combining data from the literature for field and cluster lenticulars with our data, we study correlations between parameters that characterize the bulge and the disc as a function of luminosity and environment. We find that scaling relations such as the Kormendy relation, photometric plane and other correlations involving bulge and disc parameters show a luminosity dependence. This dependence can be explained in terms of galaxy formation models in which faint lenticulars ($M_T > -24.5$) formed via secular formation processes that likely formed the pseudo-bulges of late-type disc galaxies, while brighter lenticulars ($M_T < -24.5$) formed through a different formation mechanism most likely involving major mergers. On probing variations in lenticular properties as a function of environment, we find that faint cluster lenticulars show systematic differences with respect to faint field lenticulars. These differences support the idea that the bulge and disc components fade after the galaxy falls into a cluster, while simultaneously undergoing a transformation from spiral to lenticular morphologies.

Key words: galaxies: bulges – galaxies: elliptical and lenticular – galaxies: evolution – galaxies: formation – galaxies: photometry – galaxies: structure.

1 INTRODUCTION

Lenticular (S0) galaxies were originally conceived as a morphological transition class between ellipticals and early-type spirals by Hubble (1936). These galaxies have discs spanning a wide range in luminosity, contributing between five and 50 per cent of the total galaxy light. They are distinguished from spiral galaxies by the lack of conspicuous spiral arms. For these reasons, lenticulars can be thought of as a population which is intermediate between ellipticals and early-type spirals. Indeed, the placement of lenticulars by Hubble (1936) on the tuning fork diagram clearly implies such a relationship. In several observable properties such as bulge-to-disc luminosity ratio, star formation rate and colour, lenticulars are, on average, intermediate between ellipticals and early-type spirals.

A detailed study of individual lenticular galaxies indicates that the situation is more complex in reality. It has been suggested (van den Bergh 1994) that there are different, but overlapping, subpopulations amongst the lenticulars. Exploration of formation scenarios for lenticulars using theory and numerical simulations also suggest that lenticulars may have formed in different ways. They could be of primordial origin forming rather rapidly at early epochs, or could have been formed by the slow stripping of gas from spirals, which changes the morphology (Abadi, Moore & Bower 1999), or through the mergers of unequal-mass spirals (Bekki 1998). The two main components of lenticulars – the bulge and the disc – may have their own *different* and possibly *independent* formation history. Observationally, the discs seem to be younger than the bulges in both spiral and lenticular galaxies (Peletier & Balcells 1996), with the age difference between the two components larger in lenticulars (Bothun & Gregg 1990). Bars in lenticular galaxies are also of interest in many studies as they provide a clue about the evolutionary history of these galaxies. Recent studies reveal that bars in lenticular galaxies are shorter, less massive and have smaller bar torques (Laurikainen, Salo & Buta 2005; Laurikainen et al. 2006; Buta et al. 2006; Gadotti et al. 2007).

A detailed multiband study of the morphology of representative samples of lenticulars in different environments, and comparison of their properties with those of ellipticals, and with bulges and discs of spirals, will be important in addressing these issues observationally. However, comparing the predictions of models to observations is complicated for two main reasons: (1) The

★E-mail: barway@saao.ac.za

models often use simplifying assumptions that may not hold for real galaxies and (2) models often do not make firm predictions about *directly observable* quantities. Nevertheless, the *statistical* properties of galaxy ensembles can be compared to model predictions. Such a quantitative comparison between bulge and disc properties of galaxies is considerably simplified if one assumes simple analytic profiles for the light distribution of the bulge and the disc. In practice, the Sérsic $r^{1/n}$ law (Sérsic 1968) adequately represents the bulge surface brightness distribution while an exponential best represents the disc surface brightness distribution. The total galaxy light is simply the sum of a Sérsic bulge and an exponential disc.

In this work, we obtain and report structural parameters for 36 lenticular galaxies observed in the near-infrared *K* band. Using results from the bulge–disc decomposition, we examine correlations among the bulge and disc parameters and discuss implications to models of lenticular formation. Our goal is mainly to study the constraints placed on bulge formation in lenticular galaxies by these parameter correlations. Specifically, we want to investigate, in greater detail, the discovery of Barway et al. (2007) who found two distinct populations of bulges in lenticulars that were fainter and brighter than a threshold luminosity.

This paper is organized as follows: the sample, details of near-infrared observations, data reduction technique and photometric calibration are summarized in Section 2. The 2D decomposition analysis is described in Section 3. In Section 4, we discuss the luminosity and environment dependence of lenticular galaxy properties.

Throughout this paper, we use the standard concordance cosmology with $\Omega_{\rm M} = 0.3, \Omega_\Lambda = 0.7$ and $h_{100} = 0.7$.

2 OBSERVATIONS AND DATA REDUCTION

2.1 Our sample

Our sample consists of a set of 36 bright field lenticular galaxies from Barway et al. (2005). The original sample contained 40 lenticulars galaxies, selected from the Uppsala General Catalogue (UGC), with apparent blue magnitude brighter than $m_{\rm B} = 14$, diameter $D_{25} < 3$ arcmin and declination in the range $5 < \delta < 64^\circ$. The sample, while not complete, is representative of bright field lenticulars.

We obtained images of the sample galaxies in the near infrared *K* band with the *Observatorio Astronómico Nacional* 2.1-m telescope at San Pedro Martir, Mexico. The CAMILA instrument (Cruz-Gonzalez et al. 1994), which hosts a NICMOS 3 detector of 256×256 pixel^2 format, was used in the imaging mode. Each *K* band observing sequence consisted of 10 exposures, six on the object and four on the sky. The net exposure times were, typically, 10 min per galaxy. A series of twilight and night-sky images were taken for flat-fielding purposes. The *K* observations were carried out in four runs in 2000 December, 2001 March, 2001 October and 2002 March. The data reduction procedure for the *K* images involved subtraction of the bias and sky frames, division by flat-field frames, registration of the images to a common coordinate system and then stacking of all the images of a given galaxy. All image reductions were carried out using the Image Reduction and Analysis Facility (IRAF[1]) and the Space Telescope Science Data Analysis System (STSDAS[2]). Standard fields were observed in order to enable accurate photometric calibration of our *K*-band observations. Reddening corrections due to Galactic extinction and *K*-correction were applied to individual galaxies. Full details on sample selection, observation and data reduction procedures can be found in Barway et al. (2005).

2.2 Comparison samples

We supplement our sample with data from Bedregal, Aragón-Salamanca & Merrifield (2006) (hereafter BAM06) and additional data provided by Bedregal & Aragón-Salamanca in electronic form (private communication) who used the Two Micron All Sky Survey (2MASS; Jarrett et al. 2003) data for a structural analysis of a sample of 49 lenticular galaxies. These are relatively faint objects with sufficient rotational support for the discs. Addition of these data complements our sample in two ways: (i) it provides a low-luminosity extension to the galaxies in our sample and (ii) it provides lenticulars in different environments, i.e. galaxies from the Coma (14 galaxies), Virgo (eight galaxies) and Fornax (six galaxies) clusters along with 21 field lenticulars. Whenever a comparison with other morphological classes is appropriate, we have used results from the analyses of the following samples:

(i) A sample of 42 elliptical galaxies from the Coma cluster observed in *K* band by Mobasher et al. (1999) as analysed by Khosroshahi, Wadadekar & Kembhavi (2000b).

(ii) A sample of 26 early-type spiral galaxies in the field observed by Peletier & Balcells (1997) in the *K* band as analysed by Khosroshahi et al. (2000b).

(iii) A sample of 40 late-type spiral galaxies observed and analysed by Möllenhoff & Heidt (2001) in the *K* band.

All the above analyses model the galaxy light using the Sérsic function for the bulge and an exponential function for the disc. In all cases, the bulge–disc decomposition is performed using the full 2D image of the galaxy. Incidentally, for all samples except that of BAM06 and Möllenhoff & Heidt (2001), the decomposition has been performed with the same code FITGAL (Wadadekar, Robbason & Kembhavi 1999). Details of the sample selection, observation, data reduction and bulge–disc decomposition of these samples may be found in the references cited.

3 ANALYSIS

3.1 2D image decomposition

Extracting the structural parameters of a galaxy requires the separation of the observed light distribution into bulge and disc components. There is considerable variation in the details of the decomposition techniques proposed by various researchers. In recent years, methods that employ 2D fits to broad-band galaxy images have become popular (e.g. Wadadekar, Robbason & Kembhavi 1999; Peng et al. 2002; Simard et al. 2002; de Souza, Gadotti & dos Anjos 2004). Most of these decomposition techniques assume specific surface brightness distributions like the Sérsic law for the bulge and an exponential distribution for the disc.

[1] IRAF is distributed by National Optical Astronomy Observatories, which are operated by the Association of Universities for Research in Astronomy, Inc., under cooperative agreement with the National Science Foundation.

[2] STSDAS is a product of the Space Telescope Science Institute, which is operated by AURA for NASA.

Our decomposition procedure is a full 2D method that uses information from all pixels in the image. FITGAL essentially involves a numerical solution to a signal-to-noise ratio (hereafter S/N) weighted χ^2 minimization problem. We achieve this minimization using the Davidon–Fletcher–Powell variable metric algorithm included as part of MINUIT – a multidimensional minimization package from CERN. Our technique involves iteratively building 2D image models that best fit the observed galaxy images, with the quality of the fit quantified by the χ^2 value. We compute weights for the χ^2 function using the S/N ratio at each pixel of the galaxy image. We convolve the model image with the measured point spread function (PSF) from the galaxy frame before the χ^2 is computed. Details of the accuracy and reliability of the decomposition procedure as assessed by simulations are provided in Wadadekar et al. (1999).

At near-infrared wavelengths, dust related absorption and emission from patchy star-forming regions are both weak relative to optical wavelengths. The smooth, featureless light profiles of galaxies in the near-infrared are very convenient for modelling using simple analytic functions to represent the galaxy components. Use of *K*-band data is especially important for our sample, as it includes several dusty galaxies. In our bulge–disc decomposition, we have the following quantities as free parameters: (1) $I_{\rm b}(0)$: the central bulge intensity, in counts, which can later be converted to mag arcsec^{-2} using the photometric calibration; (2) r_e: the half light radius of the bulge in pixels; (3) $e_{\rm b}$: the ellipticity of the bulge; (4) n: the bulge Sérsic index; (5) $I_{\rm d}(0)$: the central intensity of the disc in counts; (6) $r_{\rm d}$: the scalelength of the disc in pixels and (7) $e_{\rm d}$: the ellipticity of the disc.

With these definitions, the Sérsic bulge intensity distribution can be written as

$$I_{\rm bulge}(x, y) = I_{\rm b}(0)e^{-2.303b_n(r_{\rm bulge}/r_e)^{1/n}},$$
$$r_{\rm bulge} = \sqrt{x^2 + y^2/(1 - e_{\rm b})^2}, \quad (1)$$

where x and y are the distances from the centre of the galaxy along the major and minor axis, respectively and b_n is a function of n and the root of an equation involving the incomplete gamma function. However, following Khosroshahi et al. (2000b), b_n can be approximated as a linear function of n, accurate to better than one part in 10^5, by

$$b_n = 0.868242\,n - 0.142058.$$

For $n = 4$, which corresponds to the de Vaucouleurs law, $b_4 = 3.33$.

The projected disc profile is represented by an exponential distribution,

$$I_{\rm disc}(x, y) = I_{\rm d}(0)e^{-r_{\rm disc}/r_{\rm d}},$$
$$r_{\rm disc} = \sqrt{x^2 + y^2/(1 - e_{\rm d})^2}. \quad (2)$$

The ellipticity of the disc in the image is due to projection effects alone and is given by

$$e_{\rm d} = 1 - \cos(i), \quad (3)$$

where i is the angle of inclination between the line of sight and the normal to the disc plane.

The bulge-to-disc luminosity ratio is a dimensionless parameter which is commonly used as a quantitative measure for morphological classification of galaxies. For a Sérsic bulge and an exponential disc it is given by

$$(B/D)_n = \frac{n\Gamma(2n)}{(2.303b_n)^{2n}}\left[\frac{I_{\rm b}(0)}{I_{\rm d}(0)}\right]\left(\frac{r_e}{r_{\rm d}}\right)^2. \quad (4)$$

We use the bulge-to-total luminosity ratio $B/T = (B/D)/[1 + (B/D)]$ in this paper, since it spans a restricted range of 0–1.

3.2 Extraction of structural parameters using 2D image decomposition

Although the *K*-band observations are advantageous for their relative lack of absorption related problems, the high sky background in *K* band poses some difficulty in extracting the global photometric parameters accurately, as it limits the region where S/N is high enough for the pixels to be usable. Even a small error in the sky estimation can lead to spurious results because of the relatively low S/N in the images. For example, if the sky is underestimated, say by 5 per cent, the residual background can lead to a spurious detection of a large circular disc with a non-zero $I_{\rm d}(0)$. Even when a 'bulge only' model is used, a wrong assessment of the background can lead to serious misestimation of the morphological parameters.

In our *K*-band images, the sky background is automatically subtracted from the many individual sky frames for each galaxy during the preprocessing stage (see Barway et al. 2005 for details). However, if sky is removed, noise statistics calculations at low S/N (where the sky dominates) are grossly inaccurate. To avoid this problem, we added back the sky background that had been subtracted from each galaxy image.

Our bulge–disc decomposition code FITGAL (Wadadekar et al. 1999) allows the estimation of the background simultaneously with the estimation of morphological parameters. However, such a measurement can lead to unstable values for the parameters, as the background counts are much higher than the signal even in the central region of the galaxies. To avoid this instability, we had a run for each galaxy in which the aim was to estimate the background rather than to obtain the morphological parameters accurately. To this end, we first ran the code on a selected region of each galaxy image, dominated by the sky background. We compared the value of the background returned by the fitting procedure, with that estimated from regions of the image frames free of the galaxy and from the observed sky images to ensure that these values are all consistent with each other. We then adopted the sky value returned by the code as the best representation of the sky background, since this uses information from all the relevant pixels of the image, and fixed the background parameter to this value during all subsequent runs of FITGAL.

We fitted ellipses to the isophotes of each galaxy of our sample, and obtained the 1D surface brightness profile along the major axis, using the STSDAS task ELLIPSE. For this task, sky-subtracted galaxy frames were used. The fits provided us with model-independent surface brightness distributions, which could be compared to the surface brightness distribution predicted by our best-fitting bulge plus disc models. In order to obtain good initial values for our 2D fits, we fitted the inner part of 1D profiles obtained above with de Vaucouleurs law profiles (taking care to avoid the region affected by the PSF) and the outer part with the exponential law. This provided us with approximate values of $I_{\rm b}(0)$ and $r_{\rm e}$ for bulge and $I_{\rm d}(0)$ and $r_{\rm d}$ for disc, which we used as input to obtain a full 2D Sérsic and exponential model fit to each galaxy in the sample. During the fit for each galaxy, we fixed the background to the value obtained as described above. Of the 40 galaxies in our sample, we could not get satisfactory fits for three galaxies, UGC 03087, UGC 11178 and UGC 11781. UGC 03087 is a strong radio source with an optical jet visible in the image make the fit unreliable. For galaxies UGC 11178 and UGC 11781, our images suffer from poor S/N, and we are not able to get satisfactory fits. UGC 07933 is classified as an elliptical in the RC3 catalogue. We therefore exclude these four galaxies from subsequent discussions, leaving us with a sample of 36 galaxies. We

Table 1. Best-fitting bulge and disc parameters for our sample.

Name	z	T	Bulge parameters				Disc parameters			B/T	M_T
			$\mu_b(0)$ (mag arcsec^{-2})	r_e (kpc)	n	e_b	$\mu_d(0)$ (mag arcsec^{-2})	r_d (kpc)	e_d		
UGC 00080	0.01019	−3	11.54	0.45	1.63	0.001	15.69	2.33	0.505	0.19	−24.99
UGC 00491	0.01664	−1	10.38	4.95	3.82	0.257	17.65	5.08	0.231	0.65	−25.53
UGC 00859	0.00711	0	11.34	1.39	3.36	0.141	16.40	1.22	0.403	0.43	−23.25
UGC 00926	0.01467	−2.5	09.74	9.81	4.39	0.348	14.93	0.80	0.353	0.93	−26.17
UGC 01250	0.01235	−2	09.51	1.92	3.79	0.397	15.92	2.66	0.696	0.32	−25.24
UGC 01823	0.01332	−3	11.41	1.96	2.28	0.416	16.81	6.56	0.398	0.34	−26.34
UGC 01964	0.01732	−2	10.06	4.03	3.96	0.103	15.60	1.86	0.585	0.58	−25.33
UGC 02039	0.01505	−2	10.18	1.92	3.37	0.007	17.19	5.52	0.644	0.29	−25.52
UGC 02187	0.01605	−2	13.11	0.45	0.76	0.276	15.13	1.99	0.554	0.14	−25.17
UGC 02322	0.01447	−1	10.51	4.18	3.86	0.008	16.84	2.08	0.015	0.75	−24.89
UGC 03178	0.01578	−2	09.84	2.55	3.89	0.014	14.76	1.17	0.479	0.47	−24.90
UGC 03452	0.01876	−2	10.53	3.31	3.47	0.242	15.91	2.89	0.516	0.46	−25.70
UGC 03536	0.01564	−2	13.18	0.55	0.99	0.012	14.80	2.03	0.576	0.10	−25.48
UGC 03567	0.02016	−2	09.96	4.87	4.15	0.062	15.99	1.06	0.503	0.87	−25.04
UGC 03642	0.01500	−2	11.94	1.03	2.02	0.010	17.74	8.45	0.206	0.17	−25.72
UGC 03683	0.01908	−2	12.13	1.56	1.83	0.283	17.01	5.69	0.171	0.37	−25.91
UGC 03699	0.01947	−2	10.35	3.13	3.32	0.336	16.54	1.65	0.489	0.87	−25.36
UGC 03792	0.01908	0	10.17	4.41	3.74	0.224	18.15	5.71	0.225	0.72	−25.66
UGC 03824	0.01787	−2	11.40	1.52	2.71	0.003	17.43	3.18	0.002	0.52	−24.52
UGC 04347	0.01494	−2	10.68	4.33	3.34	0.243	16.34	1.01	0.528	0.95	−25.57
UGC 04767	0.02413	−2	09.05	7.65	4.74	0.105	14.98	0.27	0.001	0.99	−25.55
UGC 04901	0.02810	−2	13.30	3.06	1.78	0.305	18.08	14.28	0.043	0.27	−26.70
UGC 05292	0.00511	−2	09.22	0.26	3.08	0.008	17.28	2.01	0.282	0.21	−23.07
UGC 06013	0.02190	−2	11.29	5.10	3.68	0.325	15.41	1.00	0.001	0.78	−24.89
UGC 06389	0.00663	−2	11.71	3.00	3.36	0.378	13.88	0.21	0.334	0.89	−23.75
UGC 06899	0.02249	−2	09.79	5.11	4.06	0.060	16.71	0.53	0.001	0.99	−25.35
UGC 07142	0.00328	−2	10.48	0.35	2.22	0.219	15.96	1.32	0.503	0.33	−23.66
UGC 07473	0.00414	−2	11.76	0.24	1.20	0.239	14.55	1.20	0.725	0.12	−24.57
UGC 07880	0.00388	−3	11.50	0.68	2.39	0.330	14.29	0.63	0.747	0.34	−23.74
UGC 08675	0.00361	−2	09.18	0.25	3.35	0.020	17.14	1.48	0.011	0.19	−22.53
UGC 09200	0.01081	−2	12.33	1.35	2.23	0.117	17.83	3.10	0.001	0.57	−24.15
UGC 09592	0.01791	−2	08.69	1.62	3.62	0.315	16.30	2.33	0.123	0.65	−25.30
UGC 11356	0.00820	−2.5	11.64	0.47	1.64	0.080	15.16	1.46	0.020	0.24	−24.57
UGC 11972	0.01463	−2.5	10.29	8.62	4.08	0.441	14.24	0.45	0.002	0.95	−26.00
UGC 12443	0.01463	−2	10.83	3.34	3.44	0.097	19.36	0.04	0.002	1.00	−24.61
UGC 12655	0.01727	−2	10.34	1.14	2.87	0.191	16.86	4.77	0.400	0.24	−25.47

Notes. Column (1) gives the UGC catalogue numbers; columns (2) and (3) give redshift and morphological type respectively from NED; columns (4)–(7) give unconvolved bulge central surface brightness, bulge effective radius, the Sérsic index and bulge ellipticity, respectively; columns (8), (9) and (10) give unconvolved disc central surface brightness, disc scalelength and disc ellipticity, respectively; column (11) gives the bulge-to-total luminosity ratio and column (12) gives the absolute magnitude in the K band.

have listed in Table 1 the best-fitting bulge and disc parameters for all the 36 lenticular galaxies in the sample.

BAM06 used images in the K band from the 2MASS to obtain bulge and disc parameters for the 49 galaxies in their sample, using the GIM2D decomposition code by Simard et al. (2002), assuming Sérsic and exponential laws for the bulge and disc light distributions, as we have done with our sample. Barway et al. (2007) have shown (see their fig. 2a) that there are three clear outliers among the cluster lenticulars of the BAM06 sample. Inspection of the 2MASS K-band images of the corresponding galaxies, shows that one of these (ESO 358-G59) has poor S/N, while the other two (NGC 4638 and NGC 4787) are obviously disc-dominated systems, which are likely to have disc scalelengths larger than those reported by BAM06. Following Barway et al. (2007), we omit these three outliers from further discussion, while noting that our conclusions are not significantly changed by this omission.

It must be noted that the depth of our K-band images is considerably more than the depth of 2MASS images used by BAM06. We have a typical exposure time of 10 min per galaxy as opposed to 7.8 s per frame in 2MASS. This combined with the fact that we used a somewhat larger telescope for obtaining our data allows us to reach a depth of typically 22 mag arcsec^{-2}, corresponding to an error in photometry of 0.1 mag arcsec^{-2}. The 2MASS data used by BAM06 reach a typical depth of 20 mag arcsec^{-2} for the same error. This implies that our images are about 2 mag deeper than the 2MASS data. Given the significant difference in typical depth, bulge disc decompositions of the low S/N 2MASS data may, in principle, be systematically affected. To probe the extent of this effect, we obtained 2MASS images for all the galaxies in our sample and performed the decomposition using our technique on these data. For 80 per cent of galaxies, we found a reasonable match between parameters extracted from our data and the 2MASS data. For 20 per cent of galaxies our fitting procedure failed when using 2MASS data, indicating that the low S/N was affecting our ability to extract parameters reliably for these galaxies. However, such an inability to obtain reliable fits is unlikely to affect the parameter

extraction procedure of BAM06, which is based on the Metropolis algorithm (Metropolis et al. 1953), as implemented in the GIM2D software (Simard et al. 2002). GIM2D is a robust, albeit slow, bulge–disc decomposition software that obtains the global minimum of a fit, in almost any situation. It is thus well suited for parameter extraction for relatively shallow data like that of BAM06, where the low *S/N* is likely to make fitting difficult.

Another possible concern is whether a linear combination of a bulge and a disc is an adequate mathematical formulation to model the light distribution of galaxies in our sample, e.g. if a significant non-axisymmetric bar (or similar structure) were present for the galaxies in our sample, that would affect the parameters that we extract (see Laurikainen et al. 2005 for a discussion on the fitting of non-axisymmetric components). It is fortunately easy to detect the presence of non-axisymmetric structure by examining the residuals of our fitting, which are computed as the difference between the galaxy image and best-fitting model. Since the analytic functions we use to model the bulge and disc are axisymmetric, the bars are not modelled in our scheme. They remain in the residual image, and can be visually seen if they are bright enough. For the 36 galaxies in our sample, the RC3 catalogue indicates that five may have bars. We find from the residuals that only one galaxy (UGC 80) has a discernable bar. For the BAM06 galaxies, the RC3 catalogue indicates that 14 out of 47 galaxies may have bars. We find non-axisymmetric structures in 11 of these 15 galaxies. For these galaxies, extracted parameters are likely to be somewhat inaccurate. For the analysis subsequently reported in this paper, such inaccuracy is of concern only if it leads to *systematic* offsets between barred and non-barred galaxies. We demonstrate in Section 4.1.1 that such obvious systematic offsets do not exist, implying that inaccurate parameter estimation for a small fraction of galaxies will not alter the results of this work.

4 CORRELATIONS AND DISCUSSION

4.1 Luminosity dependence

Barway et al. (2007) have presented evidence to support the view that the formation history of lenticular galaxies depends upon their luminosity. According to this view, low-luminosity lenticular galaxies likely formed by the stripping of gas from the disc of late-type spiral galaxies, which in turn formed their bulges through secular evolution processes. On the other hand, more luminous lenticulars likely formed at early epochs through a rapid collapse followed by rapid star formation.

As we mentioned earlier, the BAM06 galaxies complement our sample in two ways: they extend to fainter luminosities and provide lenticulars in different environments. In Fig. 1, we show the distribution of total absolute magnitude ($M_{\rm T}$) in the *K* band for the combined sample, which is seen to span a wide range in luminosity. We divide the combined sample into faint and bright groups, using $M_{\rm T} = -24.5$ as a boundary. The bright sample has 37 lenticulars while 46 lenticulars belong to the faint sample according to this luminosity division. The boundary at $M_{\rm T} = -24.5$ is somewhat arbitrary but our results do not critically depend on small shifts in the dividing luminosity. For instance, changing this value by half a magnitude on either side maintains correlations significant at least at the 95 per cent level.

Using the luminosity division at $M_{\rm T} = -24.5$, Barway et al. (2007) reported markedly different correlations between bulge effective radius ($r_{\rm e}$) and disc scalelength ($r_{\rm d}$) for bright and faint lenticulars. A positive correlation of bulge and disc sizes is expected if the bulge grows over time through secular evolution processes (see review by Kormendy & Kennicutt 2004). No such correlation is expected if the bulge formed via merger-related processes. Barway et al. (2007) found this positive correlation between bulge and disc sizes of low-luminosity lenticulars; such a correlation was not observed for bright lenticulars. Moreover, they found that the correlation holds for faint galaxies, irrespective of whether they are situated in a field or cluster environment.

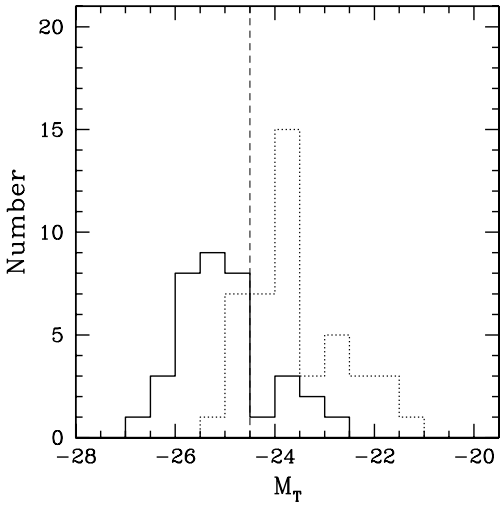

Figure 1. Distribution of total absolute magnitude (M_T) in *K* band for our sample (solid line) and for BAM06 lenticulars (dotted line). The vertical dashed line corresponds to total absolute magnitude $M_{\rm T} = -24.5$, which we use to divide low- and high-luminosity lenticulars.

If the differences between low- and high-luminosity lenticulars are indeed fundamental, then there should be systematic differences seen between the two populations in other correlations among bulge and disc parameters. We study such correlations in the following sections.

4.1.1 Kormendy relation and the effect of bars

For samples of large elliptical galaxies, the central surface brightness $\mu_{\rm b}(0)$ [or, equivalently, the mean surface brightness $\langle[\mu_{\rm b}(<r_{\rm e})]\rangle$ within $r_{\rm e}$] is correlated with $\log r_{\rm e}$. This was first reported by Kormendy (1977) and is known as the Kormendy relation. In Fig. 2(a), we show the Kormendy relation for bright (as open circles) and faint lenticulars (as filled circles). The bright lenticulars show tight correlation with the Pearson correlation coefficient $r = 0.95$ with significance greater than 99.99 per cent. The Kormendy relation for faint lenticulars shows considerably greater scatter although the Pearson correlation coefficient is 0.75 with significance greater than 99.99 per cent. Fig. 2(b) show the Kormendy relation for bright (as crosses) and faint (as dashes) lenticulars classified as barred lenticulars in RC3 catalogue to probe for any systematic effect caused due to the presence of bars. It is clear from the figure that barred and non-barred show no systematic offset. Only three galaxies are classified as barred in our bright galaxy sample (indicated by crosses). Even after removing these three galaxies, the correlation is nearly unchanged with Pearson correlation coefficient $r = 0.96$ with significance greater than 99.99 per cent. In the faint lenticular sample, there are as many as 16 galaxies classified as barred. Nevertheless, neglecting these 16 galaxies does not affect the correlation which has $r = 0.74$ with significance greater than

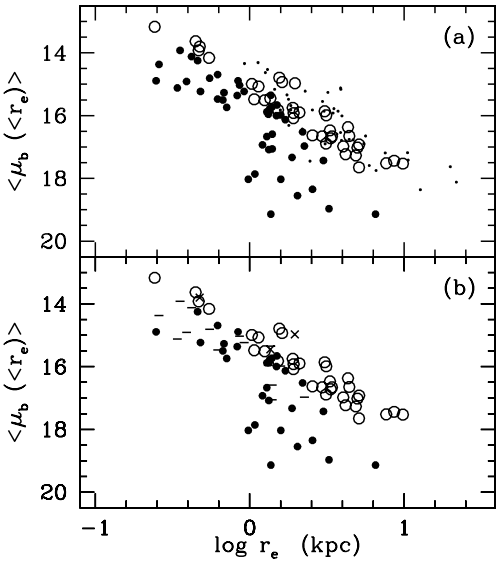

Figure 2. Dependence of the mean surface brightness within bulge effective radius ($\langle\mu_b(<r_e)\rangle$) on bulge effective radius r_e (a) for bright (as open circles) and faint lenticulars (filled circles). Coma ellipticals (as dots) are overplotted for comparison. (b) for bright lenticulars with bars (as crosses) and faint lenticulars with bars (as dashed) as classified in RC3 catalogue.

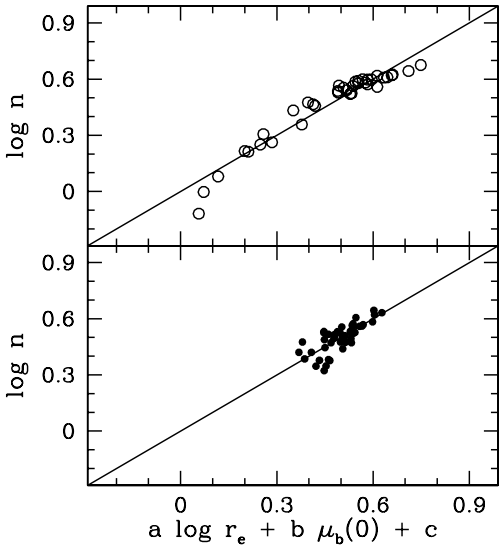

Figure 3. An edge-on view of the PP for lenticulars. Top panel: PP for bright lenticulars; $\log n = 0.251 \pm 0.045 \log r_e - 0.094 \pm 0.012\,\mu_b(0) + 1.377 \pm 0.138$. Bottom panel: PP for faint lenticulars; $\log n = 0.185 \pm 0.029, \log r_e - 0.041 \pm 0.004\,\mu_b(0) + 0.935 \pm 0.046$.

99.99 per cent. For all other correlations subsequently reported in this paper, we find that excluding barred galaxies does not significantly alter the correlation coefficient or its significance. Hence, in further discussion, we do not differentiate between barred and non-barred lenticulars, and include both types in the analysis.

The Kormendy relation is known to be a projection of the fundamental plane (FP; Djorgovski & Davis 1987; Dressler 1987) of galaxies. A tight Kormendy relation indicates (near) virialized bulges like those found in elliptical galaxies. In Fig. 2(a), ellipticals from the Coma cluster are overplotted as dots. As expected, these ellipticals show a tight correlation with Pearson correlation coefficient $r = 0.81$ with significance greater than 99.99 per cent. The slopes of the best-fitting Kormendy relation for bright lenticulars and Coma ellipticals are similar. This similarity coupled with the systematic difference in scatter in the Kormendy relation between bright and faint lenticulars is an indicator of the more virialized state of the bright lenticular bulges and their close relation to ellipticals.

4.1.2 Photometric Plane

Analogous to the FP, ellipticals and the bulges of early-type spiral galaxies obey a single planar relation of the form $\log n = a \log r_e + b\,\mu_b(0) + c$ which Khosroshahi et al. (2000a,b) called the photometric plane (PP). Assuming that galaxy bulges behave as spherical, isotropic, one-component systems, there is a unique specific entropy that can be associated with every galaxy (Lima Neto, Gerbal & Márquez 1999). This in turn implies a relation between bulge parameters that is equivalent to the observed PP. An edge-on view of the best-fitting PP is shown in the top and bottom panels of Fig. 3 for bright and faint lenticulars, respectively. Table 2 lists the coefficients for best-fitting PP relation. It is immediately evident from Fig. 3 that the PP for faint lenticulars spans a limited range of n. We restrict our bright lenticular sample to the range spanned by the faint lenticulars and then obtain the best-fitting PP for this restricted sample. The rms scatter for the (restricted) bright galaxies is considerably smaller than that for the faint galaxies (see Table 2). In Fig. 4, we show the PP for these two sets of galaxies. Visually, the higher scatter of the faint galaxies about the PP is obvious. The PP is a natural state for galaxies that formed like ellipticals (at early epochs in a burst of rapid star formation, with stellar orbits that are well relaxed). The fact that bulges of bright lenticulars have a tight PP is an indicator of homology with ellipticals. Faint lenticulars seem to belong to a separate class.

4.1.3 Correlations involving the Sérsic index (n)

The restricted range spanned by the Sérsic index in faint lenticular galaxies also affects other correlations involving this index. Fig. 5 is a plot of the Sérsic index (n) as a function of effective radius (r_e) which again shows systematic differences between bright and faint lenticulars. Bright lenticulars are well correlated having Pearson correlation coefficient $r = 0.79$ with significance greater than 99.99 per cent but faint lenticulars do not show a significant correlation. A strong correlation exists between n and the bulge central surface brightness [$\mu_b(0)$], as shown in Fig. 6 for the brighter lenticulars. The Pearson correlation coefficient in this case is 0.84 at a significance level better than 99.99 per cent. Faint lenticulars also exhibit good correlation having Pearson correlation coefficient $r = 0.58$ at significance 99.96 per cent, but have a markedly different slope. Comparing Figs 5 and 6 with figs 3 and 4, respectively, of Khosroshahi et al. (2000b), we observe a close correspondence in the distribution of the bulges of *bright* lenticulars and early-type spirals. Bulges of early-type spirals, in turn, have a close correspondence with ellipticals (Khosroshahi et al. 2000b). On the other hand, faint lenticulars seem to be a different population.

The bulge-to-total luminosity ratio (B/T) increases with the Sérsic index n as shown in Fig. 7 for brighter lenticulars ($r = 0.81$ with significance greater than 99.99 per cent). Faint lenticulars show a weak correlation between $\log (B/T)$ and $\log\ n$. Again, the trends for bright lenticulars are consistent with those found by Khosroshahi et al. (2000b) in early-type spirals. Bright lenticulars plotted in fig. 3 of Barway et al. (2007) include five galaxies that are obvious

Table 2. PP coefficients for bright and faint lenticulars.

Lenticular sample	a	b	c	N	rms_n	rms_o
Bright	0.251 ± 0.045	-0.094 ± 0.012	1.377 ± 0.138	38	0.037	0.036
Faint	0.185 ± 0.029	-0.041 ± 0.004	0.935 ± 0.046	44	0.039	0.038
Bright with restricted n	0.150 ± 0.0213	-0.056 ± 0.007	1.050 ± 0.067	29	0.019	0.019

Notes. a and b are the coefficients of $\log r_e$ and $\mu_b(0)$, respectively, c is the constant, N is the number of galaxies, rms_n is the rms scatter measured along the $\log n$ axis and rms_o is the rms scatter measured in a direction orthogonal to the best-fitting PP.

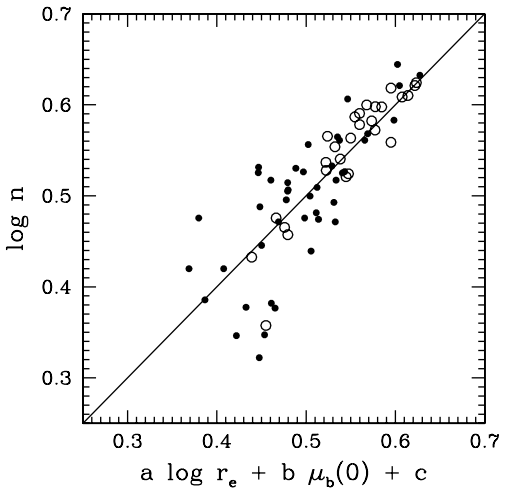

Figure 4. PP for bright lenticulars (open circles) with restricted n value. Faint lenticulars (filled circles) are over plotted on the same photometric plane. These show a higher scatter than the bright ones.

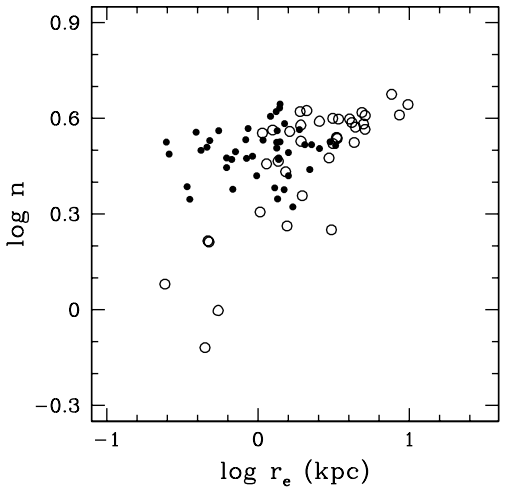

Figure 5. The Sérsic index n plotted against bulge effective radius r_e in kpc. Symbols are as in Fig. 2.

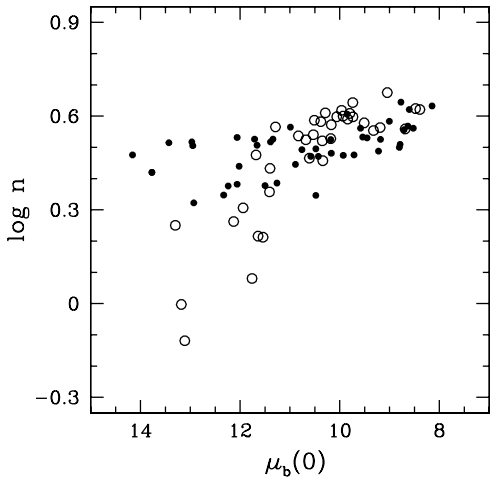

Figure 6. The Sérsic index n as a function of unconvolved bulge central surface brightness. Symbols are as in Fig. 2.

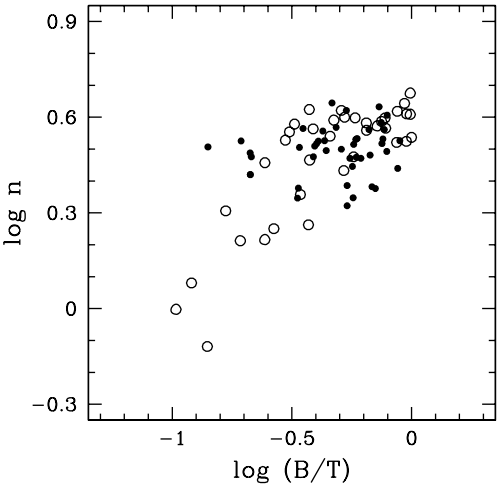

Figure 7. The Sérsic index n versus bulge-to-total luminosity ratio. Symbols are as in Fig. 2.

outliers in the anti-correlation of bulge and disc sizes. These bright lenticulars viz. UGC 80, UGC 2187, UGC 3536, UGC 7473 and UGC 11356 do follow the correlations involving the Sérsic index. However, they are all characterized by a low Sérsic index, low bulge central surface brightness, low bulge effective radius and low bulge-to-total luminosity ratio. This places these lenticulars in the bottom left quadrant of Figs 5–7. Their bulge/disc parameters indicate that these are disc-like systems, with relatively weak bulges, making them unlikely candidates of major merger induced formation. Nevertheless, they do follow the same correlations, involving the Sérsic index, as the other bright galaxies. This discrepancy needs to be explored with a larger sample of bright, but discy lenticulars.

4.1.4 Disc correlations

There exist clear correlations between the two main disc parameters – central surface brightness of the discs ($\mu_d(0)$) and disc

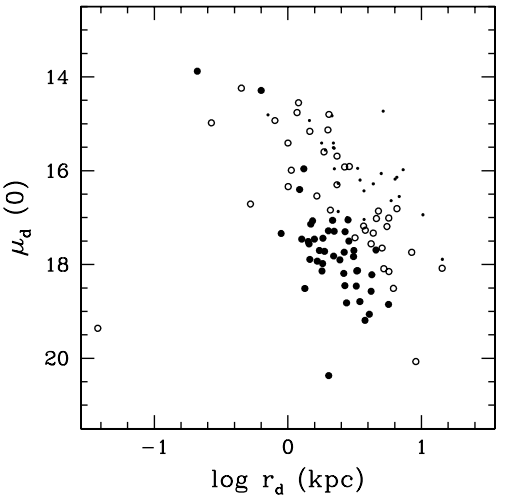

Figure 8. Unconvolved disc central surface brightness $\mu_d(0)$ as a function of disc scalelength. Early-type spirals (as dots) are overplotted for comparison. Other symbols are as in Fig. 2.

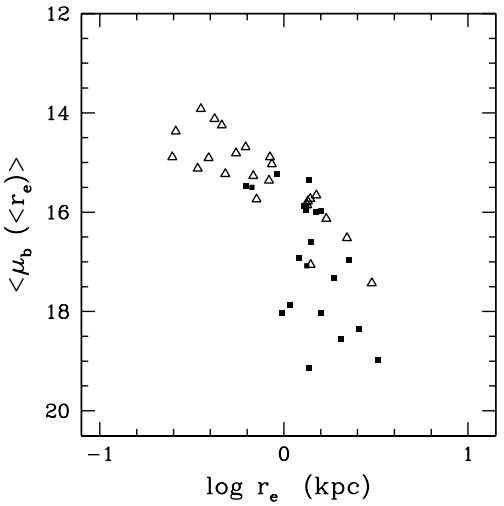

Figure 9. Dependence of the mean surface brightness within bulge effective radius ($\langle\mu_b(<r_e)\rangle$) on bulge effective radius r_e as a function of environment. Faint field lenticulars are shown as open triangles while faint cluster lenticulars are plotted as filled squares.

scalelength (r_d) – for both bright and faint lenticulars (see Fig. 8) although they occupy different regions of the plot. Lenticulars with large discs have a lower central surface brightness, on average. A clear anticorrelation is seen between these two disc parameters for bright lenticulars but the scatter is large. The linear correlation coefficient between $\mu_d(0)$ and log r_d is 0.43 with a significance of 99.37 per cent. Faint lenticulars show less scatter with the correlation coefficient of 0.70 at a significance level better than 99.99 per cent. Similar statistically significant correlation was reported by Khosroshahi et al. (2000b) for early-type spirals and Möllenhoff & Heidt (2001) for late-type spirals for these disc parameters. In Fig. 8, we also plot as dots the central surface brightness of the discs [$\mu_d(0)$] against the disc scalelength (r_d) of galaxies from the *K*-band observations of Khosroshahi et al. (2000b) of early-type spirals. From the plot it is apparent that the disc scalelengths of our sample and the Khosroshahi et al. (2000b) sample span the same range, but $\mu_d(0)$ are brighter, on the average, for early-type spirals than faint lenticulars.

4.2 Environmental dependence

The dependence of cluster environment on the formation and evolution of galaxies is well known. The environment influence is best visible through the well-known morphology–density relationship, according to which early-type galaxies are preferentially found in rich environments (Dressler 1980), with spirals are found predominately in low-density environments. One of the stronger trends seen in the morphology–density relation at low redshift is the dramatic increase in the number of lenticular galaxies in rich clusters (Dressler et al. 1997), suggesting that the dominant process in defining the morphology–density relation is the transformation of spiral galaxies into lenticular galaxies within rich clusters (Poggianti et al. 1999; Kodama & Smail 2001). These spiral galaxies are continuously supplied by accretion from the surrounding field during the course of the assembly of the cluster. *Hubble Space Telescope (HST)* imaging of 10 clusters at higher redshift ($z \sim 0.3$–0.5) by Dressler et al. (1997) shows similar behaviour. The mechanisms proposed for morphological transformation of spirals to lenticulars include dynamical interactions such as galaxy harassment (Moore et al. 1996; Moore et al. 1999; Moore, Lake & Katz 1998) and gas dynamical processes, e.g. ram pressure stripping (Abadi et al. 1999). Simulations have shown that galaxy harassment is a very efficient mechanism for transforming early-type disc galaxies to lenticulars (Moore et al. 1999) with consequent reduction in disc sizes. Ram pressure stripping truncates the star formation by removing the cold neutral gas reservoir causing the disc component of a spiral galaxy to fade within the cluster environment.

To address these possibilities observationally, it is necessary to investigate how scaling relations defined by various galaxy properties vary between field and cluster environments. In this section, we examine a few correlations as a function of environment. Unfortunately, we are unable to include bright lenticulars in this comparison because only three cluster galaxies out of the 38 in our sample are bright. For faint galaxies, the number of galaxies in the field and in clusters are almost equal, making a comparison possible.

The Kormendy relation for faint lenticulars plotted in Fig. 2 shows two distinct groups, unlike bright lenticulars. To investigate the origin of this dichotomy in the faint lenticulars, we plot the Kormendy relation for faint lenticulars, differentiating them by environment, in Fig. 9. We indicate field lenticulars with open triangles and cluster lenticulars with filled squares. The field lenticulars seem to follow the Kormendy relation reasonably well while the cluster lenticulars show a clear downward scatter with respect to the relation. On average, this requires a 1.5 mag arcsec^{-2} fading of the mean surface brightness within r_e of faint cluster lenticulars, with respect to the Kormendy relation. Boselli & Gavazzi (2006) have suggested that low-luminosity lenticulars in clusters might be the result of ram pressure stripping of late-type galaxies, which causes fading and thus lowers surface brightness.

It is interesting to see if this fading is also seen for the disc component. In Fig. 10, we plot the disc central surface brightness against the disc scalelength. As above, we indicate faint field and cluster lenticulars with different symbols. The faint field lenticulars exhibit a clear anticorrelation, whereas the cluster lenticulars occupy a limited region of the plot and show a downward scatter (indicating fading of the disc), very similar to the scatter seen in Fig. 9. Our results obtained using only photometric data are consistent with the spectroscopic results of Barr et al. (2007), which support the theory

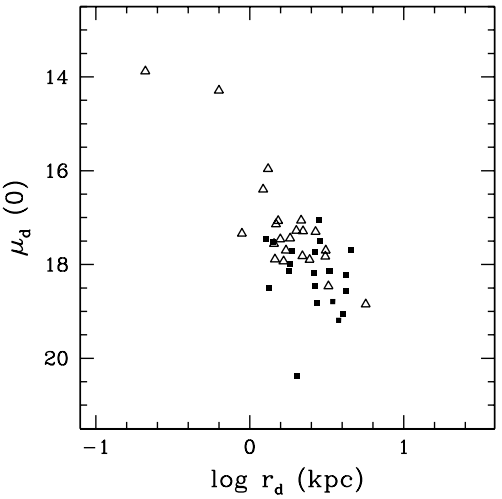

Figure 10. Unconvolved disc central surface brightness $\mu_d(0)$ is plotted against disc scalelength r_d as a function of environment. Symbols are as in Fig. 9.

that lenticular galaxies are formed when gas in normal spirals is removed (from both bulge and disc), possibly when well-formed spirals fall into the cluster. It must be noted that the sample of Barr et al. (2007) is a subset of the BAM06 sample, which is included in our analysis.

If lenticulars in clusters are indeed transformed spirals, it is likely that they preserve other signatures of their earlier existence. For instance, if they contained pseudo-bulges that formed through secular evolution, their bulge and disc sizes should be correlated (Courteau, de Jong & Broeils 1996). In Fig. 11, we plot the bulge effective radius against the disc scalelength for faint lenticulars (a similar plot for bright lenticulars may be found in Barway et al. 2007). Faint field and cluster lenticulars seem to both follow the same correlation, but inhabit different regions of the plot. We also overplot data for a sample of late-type disc galaxies from Möllenhoff & Heidt (2001). The correlation for faint lenticulars and late-type spirals has similar slopes ($\sim$1.40 $\pm$ 0.14) but different intercept which is expected as late-type spirals have larger disc scalelength compared to faint lenticulars. This is a natural expectation if late-type spirals are transforming into faint lenticulars due to an interaction with the cluster medium as well as with other galaxies in the cluster.

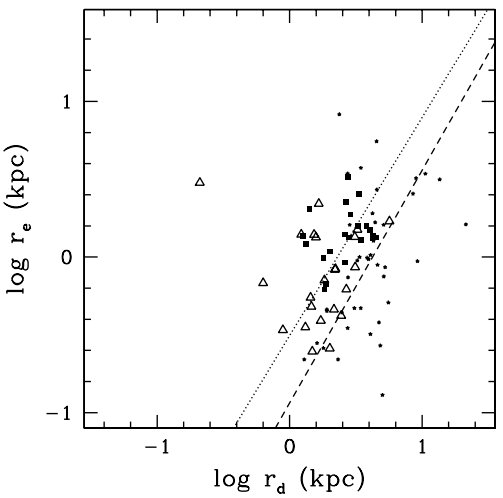

Figure 11. Dependence of the $r_e - r_d$ relation on the environment in *K* band for the faint lenticulars. Late-type spirals (as asterisks) are overplotted for comparison. Other symbols are as in Fig. 9. The dotted line is the best fit to the faint lenticulars (field as well as cluster) excluding the one obvious outlier while the dashed line is the best fit to late-type spirals. Note that these two lines have similar slopes but a different intercept.

5 SUMMARY

The main results of this paper are as follows. Several correlations such as the Kormendy relation, PP, etc. support the hypothesis that bright and faint lenticulars (in cluster or field environments) are fundamentally different, with different formation histories. Bright lenticulars resemble ellipticals and bulges of early-type spirals suggesting that they may have formed like them – at early epochs via major mergers or rapid collapse. Faint lenticulars, on the other hand, have properties consistent with them having formed via internal secular evolution processes (in the field) or via environment influenced secular evolution processes such as minor mergers, ram pressure stripping and galaxy harassment (in clusters). Although the dominant differentiating parameter between the two lenticular classes is luminosity, the environment also seems to play a role in determining the details of lenticular formation. In particular, the cluster environment seems to induce a fading of the bulge and the disc and possible transformation in morphology from spiral to lenticular, at least for the faint lenticular population.

If the formation scenario of bright and faint lenticulars is indeed completely different, it should also manifest as differences in star formation history. These differences can be probed using a combination of population synthesis models and multiband bulge disc decompositions. We intend to carry out such an analysis in a future project.

ACKNOWLEDGMENTS

We thank an anonymous referee for insightful comments that improved the content and presentation of this paper. We thank A. G. Bedregal and A. Aragón-Salamanca for providing us their bulge–disc decomposition results in electronic form. We thank Somak Raychaudhury, Swara Ravindranath, S. K. Pandey and C. D. Ravikumar for helpful discussions. This research has made use of the NASA/IPAC Extragalactic Data base (NED), which is operated by the Jet Propulsion Laboratory, California Institute of Technology, under contract with the National Aeronautics and Space Administration. This publication makes use of data products from the 2MASS, which is a joint project of the University of Massachusetts and the Infrared Processing and Analysis Center/California Institute of Technology, funded by the National Aeronautics and Space Administration and the National Science Foundation.

REFERENCES

Abadi M. G., Moore B., Bower R. G., 1999, MNRAS, 308, 947
Barr J. M., Bedregal A. G., Aragón-Salamanca A., Merrifield M. R., Bamford S. P., 2007, A&A, 470, 173
Barway S., Mayya Y. D., Kembhavi A. K., Pandey S. K., 2005, AJ, 129, 630
Barway S., Kembhavi A., Wadadekar Y., Ravikumar C. D., Mayya Y. D., 2007, ApJ, 661, L37
Bedregal A. G., Aragón-Salamanca A., Merrifield M. R., 2006, MNRAS, 373, 1125 (BAM06)
Bekki K., 1998, ApJ, 502, L133
Boselli A., Gavazzi G., 2006, PASP, 118, 517
Bothun G. D., Gregg M. D., 1990, ApJ, 350, 73

Buta R., Laurikainen E., Salo H., Block D. L., Knapen J. H., 2006, AJ, 132, 1859
Courteau S., de Jong R. S., Broeils A. H., 1996, ApJ, 457, L73
Cruz-Gonzalez I. et al., 1994, RMxAA, 29, 197
Djorgovski S., Davis M., 1987, ApJ, 313, 59
Dressler A., 1980, ApJ, 236, 351
Dressler A., Lynden-Bell D., Burstein D., Davies R. L., Faber S. M., Terlevich R., Wegner G., 1987, ApJ, 313, 42
Dressler A. et al., 1997, ApJ, 490, 577
Gadotti D. A., Athanassoula E., Carrasco L., Bosma A., de Souza R. E., Recillas E., 2007, MNRAS, 381, 943
Hubble E. P., 1936, The Realm of the Nebulae. Yale Univ. Press, New Haven
Jarrett T. H., Chester T., Cutri R., Schneider S. E., Huchra J. P., 2003, AJ, 125, 525
Khosroshahi H. G., Wadadekar Y., Kembhavi A., Mobasher B., 2000a, ApJ, 531, L103
Khosroshahi H. G., Wadadekar Y., Kembhavi A., 2000b, ApJ, 533, 162
Kodama T., Smail I., 2001, MNRAS, 326, 637
Kormendy J., 1977, ApJ, 218, 333
Kormendy J., Kennicutt R. C. Jr., 2004, ARA&A, 42, 603
Laurikainen E., Salo H., Buta R., 2005, MNRAS, 362, 1319
Laurikainen E., Salo H., Buta R., Knapen J., Speltincx T., Block D., 2006, AJ, 132, 2634
Lima Neto G. B., Gerbal D., Márquez I., 1999, MNRAS, 309, 481
Metropolis N., Rosenbluth N., Rosenbluth A., Teller A., Teller E., 1953, J. Chem. Phys., 21, 1087
Mobasher B., Guzman R., Aragón-Salamanca A., Zepf S., 1999, MNRAS, 304, 225
Möllenhoff C., Heidt J., 2001, A&A, 368, 16
Moore B., Katz N., Lake G., Dressler A., Oemler A., 1996, Nat, 379, 613
Moore B., Lake G., Katz N., 1998, ApJ, 495, 139
Moore B., Lake G., Quinn T., Stadel J., 1999, MNRAS, 304, 465
Peletier R. F., Balcells M., 1996, AJ, 111, 2238
Peletier R. F., Balcells M., 1997, New Astron. 1, 349
Peng C. Y., Ho L. C., Impey C. D., Rix H., 2002, AJ, 124, 266
Poggianti B. M., Smail I., Dressler A., Couch W. J., Barger A. J., Butcher H., Ellis R. S., Oemler A. J., 1999, ApJ, 518, 576
Simard L. et al., 2002, ApJS, 142, 1
Sérsic J. L., 1968, Atlas de Galaxias Australes. Obs. Astron. Cordoba
de Souza R. E., Gadotti D. A., dos Anjos S., 2004, ApJS, 153, 411
van den Bergh S., 1994, AJ, 107, 153
Wadadekar Y., Robbason B., Kembhavi A., 1999, AJ, 117, 1219

This paper has been typeset from a TEX/LATEX file prepared by the author.